

Effect of Surface Reconstruction on Molecular Chemisorption: A Scanning Tunneling Microscopy Study of $\text{H}_8\text{Si}_8\text{O}_{12}$ Clusters on $\text{Au}(111) 23 \times \sqrt{3}$

Kevin S. Schneider,[†] Kenneth T. Nicholson,[†] Daniel R. Fosnacht,[†]
Bradford G. Orr,^{*,‡} and Mark M. Banaszak Holl^{*,†}

Chemistry Department, University of Michigan, Ann Arbor, Michigan 48109-1055, and
Physics Department and the Applied Physics Program, University of Michigan,
Ann Arbor, Michigan 48109-1120

Received July 17, 2002

Scanning tunneling microscopy (STM) data are presented in conjunction with reflection–absorption infrared spectroscopy and X-ray photoemission spectroscopy data investigating the adsorbate layer formation of $\text{H}_8\text{Si}_8\text{O}_{12}$ clusters on a clean $\text{Au}(111) 23 \times \sqrt{3}$ surface. All three experimental techniques independently support desorption of approximately 10–15% of the $\text{H}_8\text{Si}_8\text{O}_{12}$ clusters from the $\text{Au}/\text{H}_7\text{Si}_8\text{O}_{12}$ adsorbate layer surface following evacuation of excess $\text{H}_8\text{Si}_8\text{O}_{12}$ cluster pressure from the ultrahigh vacuum reaction chamber. Surprisingly, the STM data indicate that unlike all other reported molecular adsorbates having a strong chemical interaction with the $\text{Au}(111)$ surface, the $23 \times \sqrt{3}$ surface reconstruction is preserved following chemisorption of $\text{H}_8\text{Si}_8\text{O}_{12}$ clusters. Additionally, at saturation coverage the clusters are preferentially bound to, and predominantly desorb from, specific sites on the $\text{Au}(111) 23 \times \sqrt{3}$ reconstructed surface. The preferential cluster adsorption/desorption behavior creates a unique pattern of holes and channels in the $\text{Au}/\text{H}_7\text{Si}_8\text{O}_{12}$ adsorbate layer surface.

Introduction

$\text{Au}(111)$ adopts a $23 \times \sqrt{3}$ surface reconstruction in order to reduce surface free energy.^{1–5} The surface consists of hexagonally close-packed (hcp) and face-centered cubic (fcc) regions connected by transitional bridge sites elevated ~ 0.2 Å relative to the fcc regions (Figure 1). Frequently, the surface reconstruction is broken upon the addition of molecular adsorbates. Alkanethiols ($\text{CH}_3(\text{CH}_2)_n\text{SH}$), a widely studied example, are known to strongly interact with the substrate, relax the $23 \times \sqrt{3}$ surface reconstruction, and pack alkyl chains to form a self-assembled monolayer or two-dimensional crystal.^{6–8} Conversely, the polycyclic aromatic 3,4,9,10-perylenetetracarboxylic-dianhydride (PTCDA) forms a well-ordered array that leaves the $\text{Au}(111) 23 \times \sqrt{3}$ surface reconstruction intact.^{9–11} However, the molecule–substrate interactions for this system appear quite small and identical PTCDA adsorbate packing is observed on many other surfaces including graphite,^{12–16} $\text{InAs}(001)$,¹⁷ $\text{GaAs}(001)$,¹⁸ $\text{Ag}(111)$, and $\text{Ag}(110)$.^{19–21} Weakly physisorbed molecules and noble gases have been observed to form ordered phases, includ-

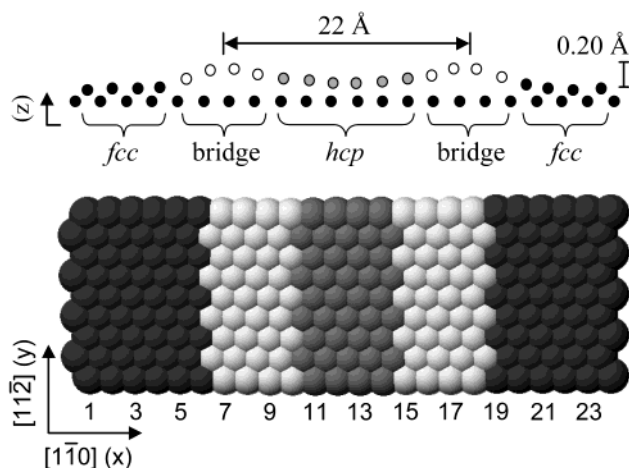


Figure 1. Model of the $\text{Au}(111) 23 \times \sqrt{3}$ surface. Atoms are color-coded as follows: regions of ABC (fcc) and ABA (hcp) stacking are black and gray, respectively, with transition (bridge) regions (between fcc and hcp) colored white.

ing herringbone structures, on a number of surfaces.²² Additionally, quasi-patterned submonolayer metal films

[†] Chemistry Department.

[‡] Physics Department and the Applied Physics Program.

(1) Van Hove, M. A.; Koestner, R. J.; Stair, P. C.; Bibérian, J. P.; Kresmodel, L. L.; Bartoš, I.; Somorjai, G. A. *Surf. Sci.* **1981**, *103*, 189.

(2) Harten, U.; Lahee, A. M.; Toennies, J. P.; Wöll, C. *Phys. Rev. Lett.* **1985**, *54*, 2619.

(3) Wöll, C.; Chiang, S.; Wilson, R. J.; Lippel, P. H. *Phys. Rev. B* **1989**, *39*, 7988.

(4) Barth, J. V.; Brune, H.; Ertl, G.; Behm, R. J. *Phys. Rev. B* **1990**, *42*, 9307.

(5) Chambliss, D. D.; Wilson, R. J.; Chiang, S. *J. Vac. Sci. Technol., B* **1991**, *9*, 933.

(6) Poirier, G. E.; Pylant, E. D. *Science* **1996**, *272*, 1145.

(7) Poirier, G. E. *Langmuir* **1997**, *13*, 2019.

(8) Poirier, G. E. *Chem. Rev.* **1997**, *97*, 1117.

(9) Fenter, P.; Schreiber, F.; Zhou, L.; Eisenberger, P.; Forrest, S. R. *Phys. Rev. B* **1997**, *56*, 3046.

(10) Schmitz-Hubsch, T.; Fritz, T.; Sellam, F.; Staub, R.; Leo, K. *Phys. Rev. B* **1997**, *55*, 7972.

(11) Chizhov, I.; Kahn, A.; Scoles, G. *J. Cryst. Growth* **2000**, *208*, 449.

(12) Forrest, S. R.; Kaplan, M. L.; Schmidt, P. H. *Annual Review of Materials Science*; Huggins, R. A., Ed.; Annual Reviews, Inc.: Palo Alto, CA, 1987; Vol. 17, p 189.

(13) Ludwig, C.; Gompf, J.; Glatz, W.; Petersen, J.; Eisenmenger, W.; Moblus, M.; Karl, N. *Z. Phys. B* **1992**, *86*, 397.

(14) Ludwig, C.; Gompf, J.; Petersen, J.; Strohmaier, R.; Eisenmenger, W. *Z. Phys. B* **1994**, *93*, 365.

(15) Forrest, S. R.; Burrows, P. E.; Haskal, E. I.; So, F. F. *Phys. Rev. B* **1994**, *49*, 11309.

(16) Kendrick, C.; Kahn, A.; Forrest, S. R. *Appl. Surf. Sci.* **1996**, *104/105*, 586.

(17) Kendrick, C.; Kahn, A. *J. Cryst. Growth* **1997**, *181*, 181.

(18) Hirose, Y.; Forrest, S. R.; Kahn, A. *Phys. Rev. B* **1995**, *52*, 14040.

(19) Seidel, C.; Awater, C.; Liu, X. D.; Ellerbrake, R.; Fuchs, H. *Surf. Sci.* **1997**, *371*, 123.

(20) Glöcker, K.; Seidel, C.; Soukopp, A.; Sokolowski, M.; Umbach, E.; Böhringer, M.; Berndt, R.; Schneider, W. D. *Surf. Sci.* **1998**, *405*, 1.

(21) Böhringer, M.; Schneider, W. D.; Berndt, R.; Glöcker, K.; Sokolowski, M.; Umbach, E. *Phys. Rev. B* **1998**, *57*, 4081.

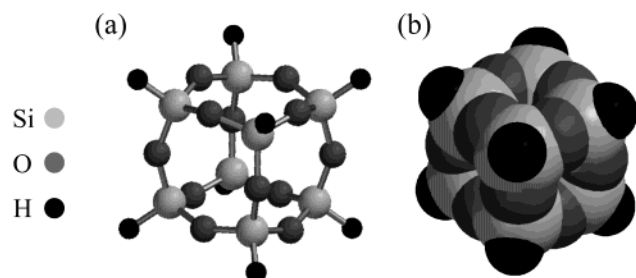


Figure 2. $\text{H}_8\text{Si}_8\text{O}_{12}$: (a) ball and stick model and (b) space filling model. Silicon, oxygen, and hydrogen atoms occupy cluster corners, edges, and corner vertices, respectively.

grown on Au(111) $23 \times \sqrt{3}$ have been observed for a variety of metals.^{5,23–25} However, to the best of our knowledge, molecules having strong *covalent* interactions with the surface have not been observed to pattern on the $23 \times \sqrt{3}$ gold surface reconstruction in this fashion. Surprisingly, the chemisorption of $\text{H}_8\text{Si}_8\text{O}_{12}$ with Au(111) $23 \times \sqrt{3}$ occurs via covalent Au–Si bond formation and exhibits important cluster–cluster interactions, yet the $23 \times \sqrt{3}$ surface reconstruction is maintained.

The chemisorption of $\text{H}_8\text{Si}_8\text{O}_{12}$ clusters to freshly evaporated Au(111) surfaces has been previously reported.^{26–29} Characterization by X-ray photoemission spectroscopy (XPS) and reflection–absorption infrared spectroscopy (RAIRS) provides strong evidence for the formation of a new Au–Si bond yielding a chemisorbed adsorbate layer comprised of single-vertex attached clusters. Other key points of the previous studies include the ambient temperature reversible Si–H bond activation by the gold surface, the formation of a spectroscopically (XPS and RAIRS) homogeneous Au/ $\text{H}_7\text{Si}_8\text{O}_{12}$ adsorbate structure, and a dynamic adsorption and exchange process characterized by a precursor kinetic model. Indirect spectroscopic and chemical evidence implied the presence of holes in the Au/ $\text{H}_7\text{Si}_8\text{O}_{12}$ adsorbate layer that mediated the exchange process. However, direct evidence of these holes was lacking and the size, shape, and local structure of the gold surface at these sites could not be determined from the spectroscopic data. In addition, the effect of the adsorbate upon the gold surface reconstruction and the arrangement of the clusters on the surface were not addressed.

In this paper, scanning tunneling microscopy (STM) images are presented, in conjunction with RAIRS and XPS data, highlighting an unexpected discovery of preferential binding sites for $\text{H}_8\text{Si}_8\text{O}_{12}$ (Figure 2) to the maintained Au(111) $23 \times \sqrt{3}$ surface reconstruction. All three surface characterization techniques independently support desorption of approximately 10–15% of the $\text{H}_8\text{Si}_8\text{O}_{12}$ clusters from the Au/ $\text{H}_7\text{Si}_8\text{O}_{12}$ adsorbate layer surface upon evacuation of clusters from the ultrahigh vacuum (UHV) reaction chamber. Analysis of the STM data yields two surprising results: (1) the Au(111) $23 \times \sqrt{3}$ surface re-

construction is *preserved* following chemisorption of $\text{H}_8\text{Si}_8\text{O}_{12}$ and (2) at saturation coverage, the $\text{H}_8\text{Si}_8\text{O}_{12}$ clusters are preferentially bonded to bridge and hcp sites (and thus more readily desorb from the fcc sites) intrinsic to the Au(111) $23 \times \sqrt{3}$ surface. The reaction of $\text{H}_8\text{Si}_8\text{O}_{12}$ with Au(111) $23 \times \sqrt{3}$ represents a unique example in which the $23 \times \sqrt{3}$ surface reconstruction is preserved following the formation of a covalently bound adsorbate layer. Additionally, the site-specific cluster adsorption/desorption behavior yields a discontinuous Au/ $\text{H}_7\text{Si}_8\text{O}_{12}$ adsorbate layer surface containing a complex pattern of holes and channels. The holes present in the discontinuous adsorbate layer may provide an avenue for, or facilitate, known $\text{H}_8\text{Si}_8\text{O}_{12}/\text{H}_8\text{Si}_8\text{O}_{12}$, $\text{H}_8\text{Si}_8\text{O}_{12}/\text{D}_8\text{Si}_8\text{O}_{12}$, and $\text{H}_8\text{Si}_8\text{O}_{12}/\text{C}_6\text{H}_{13}\text{H}_7\text{Si}_8\text{O}_{12}$ cluster exchange reactions.^{28,29} These novel surface structures and their relationship to cluster adsorption and desorption are the focus of this paper.

Understanding molecular adsorption onto surfaces can provide knowledge about fundamental formation processes for both amorphous and crystalline interfaces. To gain a theoretical understanding and develop practical systems in such disparate areas as catalysis, corrosion protection, and dielectric film growth, researchers have employed a variety of molecules as adsorbates. One-dimensional reagents such as alkanethiols and two-dimensional reagents such as polycyclic aromatics have proven especially useful.³⁰ Such studies have allowed detailed structural models of adsorbate binding and packing to be proposed. Far fewer reports have appeared describing the more topologically complex case of three-dimensional cage molecules. Single and multilayer coverages of polyoxoanions (POA),^{31–33} fullerenes,^{34–39} metal halides,^{40,41} polyhedral borane,⁴² and hydridosilsesquioxane clusters such as $\text{H}_8\text{Si}_8\text{O}_{12}$ ^{26,28,29,43–47} have all been described. In these cases, the local cluster registry with the surface has been reported only for the POA^{48,49} and $\text{H}_8\text{Si}_8\text{O}_{12}$ cases.^{26,28,29,43–47} To our knowledge, long-range cluster–cluster packing and ordering has been reported only for the POA systems.

(30) Ulman, A. *Chem. Rev.* **1996**, *96*, 1533.

(31) Keita, B.; Nadjjo, L. *Surf. Sci. Lett.* **1991**, *254*, L443.

(32) Keita, B.; Chauveau, F.; Theobald, F.; Belanger, D.; Nadjjo, L. *Surf. Sci.* **1992**, *264*, 271.

(33) Keita, B.; Nadjjo, L. *J. Electroanal. Chem.* **1993**, *354*, 295.

(34) Altman, E. I.; Colton, R. J. *Surf. Sci.* **1992**, *279*, 49.

(35) Altman, E. I.; Colton, R. J. *Surf. Sci.* **1993**, *295*, 13.

(36) Gimzewski, J. K.; Modesti, S.; Schlittler, R. R. *Phys. Rev. Lett.* **1994**, *72*, 1036.

(37) Gimzewski, J. K.; Modesti, S.; Gerber, C.; Schlittler, R. R. *Chem. Phys. Lett.* **1993**, *213*, 401.

(38) Johansson, M. K.-J.; Maxwell, A. J.; Gray, S. M.; Brühwiler, P. A.; Mancini, D. C.; Johansson, L. S. O.; Mårtensson, N. *Phys. Rev. B* **1996**, *54*, 13472.

(39) Maxwell, A. J.; Brühwiler, P. A.; Andersson, S.; Arvanitis, D.; Hernnäs, B.; Karis, O.; Mancini, D. C.; Mårtensson, N.; Gray, S. M.; Johansson, M. K.-J.; Johansson, L. S. O. *Phys. Rev. B* **1995**, *52*, R5546.

(40) Prokopuk, N.; Shriver, D. F. *Chem. Mater.* **1998**, *10*, 10.

(41) Prokopuk, N.; Shriver, D. F. *Chem. Mater.* **1999**, *11*, 1230.

(42) Yeager, L. J.; Saeki, F.; Shelly, K.; Hawthorne, M. F.; Garrell, R. L. *J. Am. Chem. Soc.* **1998**, *120*, 9961.

(43) Lee, S.; Makan, S.; Banaszak Holl, M. M.; McFeely, F. R. *J. Am. Chem. Soc.* **1994**, *116*, 11819.

(44) Banaszak Holl, M. M.; McFeely, F. R. *Phys. Rev. Lett.* **1993**, *71*, 2441.

(45) Greeley, J. N.; Banaszak Holl, M. M. *Inorg. Chem.* **1998**, *37*, 6014.

(46) Greeley, J. N.; Meeuwenberg, L. M.; Banaszak Holl, M. M. *J. Am. Chem. Soc.* **1998**, *120*, 7776.

(47) Schneider, K. S.; Zhang, Z.; Banaszak Holl, M. M.; Orr, B. G.; Pernisz, U. C. *Phys. Rev. Lett.* **2000**, *85*, 602.

(48) Ge, M. H.; Zhong, B. X.; Klemperer, W. G.; Gewirth, A. A. *J. Am. Chem. Soc.* **1996**, *118*, 5812.

(49) Lee, L.; Wang, J. X.; Adzic, R. R.; Robinson, I. K.; Gewirth, A. A. *J. Am. Chem. Soc.* **2001**, *123*, 8838.

(22) Somorjai, G. A. *Introduction to surface chemistry and catalysis*; John Wiley & Sons: New York, 1994; p 72.

(23) Chambliss, D. D.; Wilson, R. J. *J. Vac. Sci. Technol., B* **1991**, *9*, 928.

(24) Strocio, J. A.; Pierce, D. T.; Dragoset, R. A.; First, P. N. *J. Vac. Sci. Technol., A* **1992**, *10*, 1981.

(25) Barth, J. V.; Behm, R. J.; Ertl, G. *Surf. Sci.* **1995**, *341*, 62.

(26) Nicholson, K. T.; Zhang, K. Z.; Banaszak Holl, M. M. *J. Am. Chem. Soc.* **1999**, *121*, 3232.

(27) Nicholson, K. T.; Biscotto, M. A.; Banaszak Holl, M. M. *Mater. Res. Soc. Symp. Proc.* **1999**, *567*, 543.

(28) Nicholson, K. T.; Zhang, K. Z.; Banaszak Holl, M. M.; McFeely, F. R.; Pernisz, U. C. *Langmuir* **2000**, *16*, 8396.

(29) Nicholson, K. T.; Zhang, K. Z.; Banaszak Holl, M. M.; McFeely, F. R.; Calzaferrri, G.; Pernisz, U. C. *Langmuir* **2001**, *17*, 7879.

Experimental Section

$\text{H}_8\text{Si}_8\text{O}_{12}$ was synthesized by the method of Agaskar and sublimed twice.^{50,51} $\text{C}_6\text{H}_{13}\text{-H}_7\text{Si}_8\text{O}_{12}$ was prepared by literature procedures.^{52,53} Cluster purity was checked using ^1H NMR, IR, and gas chromatography–mass spectrometry (GC–MS). After the individual cluster samples were loaded into separate glass or steel UHV-compatible sample containers, the samples were further purified by sublimation, via gentle heating in a water bath at $\sim 50^\circ\text{C}$ and prolonged (>24 h) exposure to pumping, in UHV conditions.

Clean Au(111) samples for STM imaging experiments were prepared by in situ annealing of a commercially fabricated sample of Au deposited on mica (Molecular Imaging) in UHV (base pressure, 5×10^{-11} Torr). Sample annealing was accomplished by resistively heating to $\sim 400\text{--}500^\circ\text{C}$ a $\sim 3\text{ mm} \times 5\text{ mm} \times 0.3\text{ mm}$ piece of Si(100) situated directly underneath the mica. In a separate chamber (base pressure, 3×10^{-10} Torr), gold (99.999% vacuum deposition grade, Cerac, Inc., placed inside a coiled tungsten filament) was deposited on the surface and the sample was further annealed for at least 1 h. Prior to cluster adsorption, Au samples were imaged in UHV (base pressure, 5×10^{-11} Torr) by STM in order to gauge the overall sample cleanliness and confirm the presence of the Au(111) $23 \times \sqrt{3}$ surface reconstruction. Room-temperature constant-current images were obtained using an RHK Technology, Inc. UHV300 series variable temperature STM at typical sample biases (V_s) of -0.5 to -1.0 V and tunneling currents (I_t) of $0.2\text{--}3.0\text{ nA}$. Low or high pass filtering was employed to attenuate extraneous noise in the STM images and is noted where appropriate.

Gold samples for RAIRS and XPS experiments were prepared by first evaporating either Cr or Ti onto an oxidized Si(100)- 2×1 sample, for use as an adhesion layer, followed by at least 1000 Å of Au. Immediately prior to use, additional gold was evaporated onto the surface in UHV and sample purity was assessed by XPS. Only trace amounts of carbon impurities could be detected. RAIRS experiments were performed with a Bio-Rad FTS-40 FTIR spectrometer. XPS experiments were performed with a PHI5000C spectrometer. Complete details of the photoemission chamber and RAIRS experimental apparatus have been fully described elsewhere.^{43,46}

Clusters were introduced into the UHV chambers via a leak valve. Au(111) samples for STM experiments were dosed with a saturation coverage (typically $10\text{--}500$ langmuir; 1 langmuir = 1×10^{-6} Torr·s) of gaseous $\text{H}_8\text{Si}_8\text{O}_{12}$ at room temperature at a pressure of 4×10^{-7} Torr. Au(111) samples for RAIRS and XPS experiments were dosed with a saturation coverage of $\text{H}_8\text{Si}_8\text{O}_{12}$ at room temperature at a pressure of 4×10^{-8} Torr. For the $\text{H}_8\text{Si}_8\text{O}_{12}/\text{C}_6\text{H}_{13}\text{-H}_7\text{Si}_8\text{O}_{12}$ mixed-cluster-layer XPS experiments, $\text{C}_6\text{H}_{13}\text{-H}_7\text{Si}_8\text{O}_{12}$ was dosed at room temperature at a pressure of 1×10^{-8} Torr until saturation coverage was achieved. Due to the decreased volatility of $\text{C}_6\text{H}_{13}\text{-H}_7\text{Si}_8\text{O}_{12}$ (relative to $\text{H}_8\text{Si}_8\text{O}_{12}$), the material was heated to $\sim 50^\circ\text{C}$ in a water bath in order to obtain an adequate vapor pressure. Details of the $\text{H}_8\text{Si}_8\text{O}_{12}/\text{C}_6\text{H}_{13}\text{-H}_7\text{Si}_8\text{O}_{12}$ mixed-cluster-layer formation reactions have been described elsewhere.²⁹

For RAIRS experiments, clean gold background spectra were acquired prior to introduction of clusters into the chamber. Following cluster exposure, two types of “sample sets” were collected: (1) in the presence of a cluster overpressure (i.e., clusters were being actively introduced into the chamber) and (2) following evacuation of the cluster overpressure from the chamber ($\leq 1 \times 10^{-9}$ Torr). Each scan set consisted of 100 scans at 8 cm^{-1} resolution.

Matlab v4.2c was employed for curve fitting the STM height histogram and XPS data. For both the STM height histogram and full-coverage XPS data, curve fitting was performed in which peak height, position, and width were allowed to vary. The WIN-IR program for Microsoft Windows 3.0 was used for integration of IR data.

(50) Agaskar, P. A. *Inorg. Chem.* **1991**, *30*, 2707.

(51) Agaskar, P. A.; Klemperer, W. G. *Inorg. Chim. Acta* **1995**, *229*, 355.

(52) Calzaferri, G.; Imhof, R.; Tornroos, K. W. *J. Chem. Soc., Dalton Trans.* **1994**, 3123.

(53) Marcolli, C.; Calzaferri, G. *Appl. Organomet. Chem.* **1999**, *13*, 213.

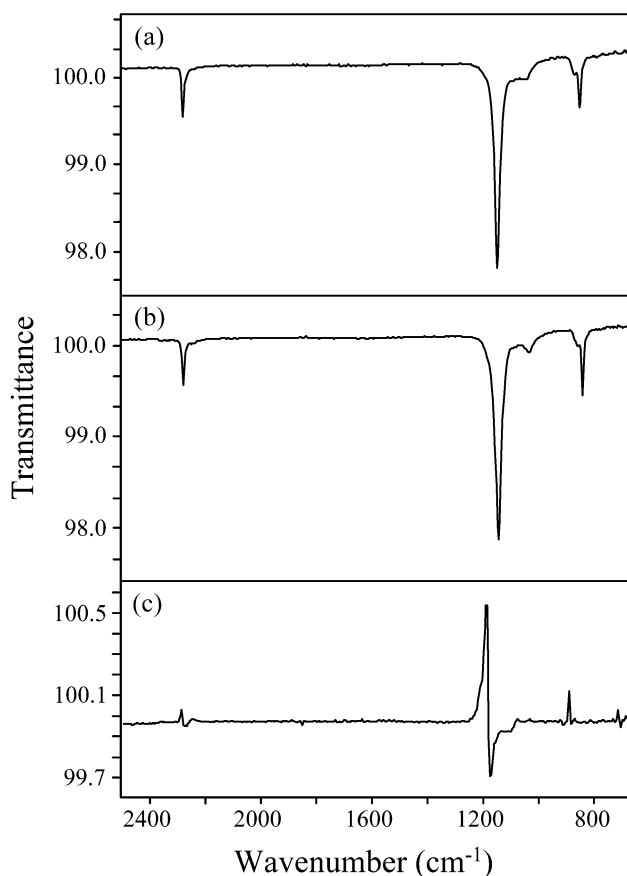


Figure 3. (a) RAIRS of a layer of $\text{H}_8\text{Si}_8\text{O}_{12}$ chemisorbed to freshly evaporated gold in the presence of a cluster overpressure of 4×10^{-8} Torr. (b) RAIRS of a layer of $\text{H}_8\text{Si}_8\text{O}_{12}$ chemisorbed to gold with no cluster overpressure. (c) Difference spectrum of (a) and (b) where the chemisorbed layer of $\text{H}_8\text{Si}_8\text{O}_{12}$ on gold in the presence of cluster overpressure (spectrum a) is employed for the background subtraction.

Results and Discussion

I. RAIRS Data. RAIRS spectra of saturating doses of $\text{H}_8\text{Si}_8\text{O}_{12}$ on clean Au(111) in the presence of 4×10^{-8} Torr cluster overpressure and without a cluster overpressure (7×10^{-10} Torr) are presented in Figure 3a,b. Spectrum 3a shows intense features at approximately 889 , 1185 , and 2281 cm^{-1} assigned as $\delta(\text{Si-H})$, $\nu_{\text{as}}(\text{Si-O-Si})$, and $\nu(\text{H-SiO}_3)$, respectively. These assignments are based on IR data collected for $\text{H}_8\text{Si}_8\text{O}_{12}$ clusters,^{52,54} $\text{H}_8\text{Si}_8\text{O}_{12}$ chemisorbed to Si(100)- 2×1 ,^{46,55} $\text{D}_8\text{Si}_8\text{O}_{12}$ chemisorbed to Si(100)- 2×1 ,⁴⁶ solution data for $\text{RH}_7\text{Si}_8\text{O}_{12}$ clusters,⁵³ and density functional theory calculations modeling $\text{H}_8\text{Si}_8\text{O}_{12}$ chemisorption to a Si(100)- 2×1 surface dimer.⁵⁶ A nearly identical spectrum is obtained following evacuation of the $\text{H}_8\text{Si}_8\text{O}_{12}$ cluster overpressure from the UHV chamber (Figure 3b). However, upon closer inspection the $\delta(\text{Si-H})$ and $\nu_{\text{as}}(\text{Si-O-Si})$ peaks have shifted to lower energies by approximately 2 and 4 cm^{-1} , respectively. The cluster overpressure dependency of the $\delta(\text{Si-H})$ and $\nu_{\text{as}}(\text{Si-O-Si})$ frequency shifts has been previously observed and primarily attributed to anomalous dispersion and vibrational coupling.^{28,29} Figure 3c plots the difference of spectra

(54) Bartsch, M.; Bornhauser, P.; Calzaferri, G.; Imhof, R. *J. Phys. Chem.* **1994**, *98*, 2817.

(55) Eng, J., J.; Raghavachari, K.; Struck, L. M.; Chabal, Y. J.; Bent, B. E.; Banaszak Holl, M. M.; McFeely, F. R.; Michaels, A. M.; Flynn, G. W.; Christman, S. B.; Chaban, E. E.; Williams, G. P.; Radermacher, K.; Mantl, S. *J. Chem. Phys.* **1998**, *108*, 8680.

(56) Nicholson, K. T.; Banaszak Holl, M. M. *Phys. Rev. B* **2001**, *64*, 155317.

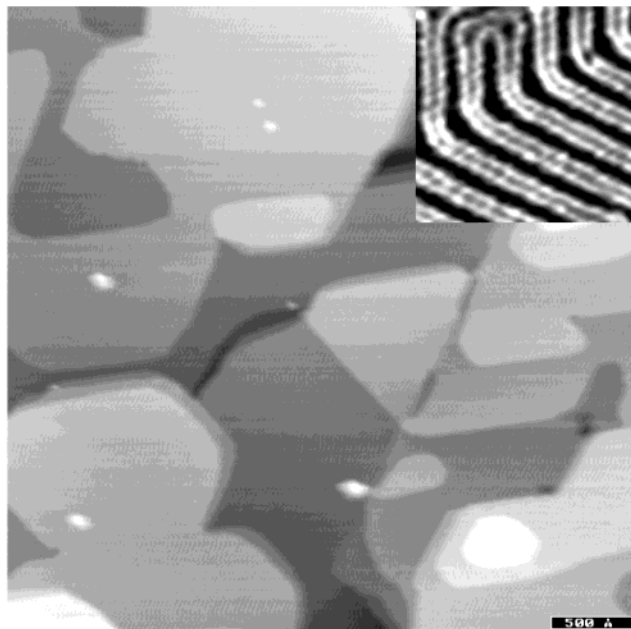


Figure 4. Typical clean gold sample, $4000 \text{ \AA} \times 4000 \text{ \AA}$. Inset: $400 \text{ \AA} \times 400 \text{ \AA}$ high-resolution image clearly displaying the Au(111) $23 \times \sqrt{3}$ herringbone surface reconstruction.

a and b in which the chemisorbed layer of $\text{H}_8\text{Si}_8\text{O}_{12}$ on gold in the presence of a cluster overpressure (spectrum a) is employed for the background subtraction. The difference spectrum, spectrum c, clearly displays an approximate 5–10% decrease in $\delta(\text{Si-H})$, $\nu_{\text{as}}(\text{Si-O-Si})$, and $\nu(\text{H-SiO}_3)$ signal peak intensities upon evacuation of cluster overpressure. This is suggestive of desorption of 5–10% of the $\text{H}_8\text{Si}_8\text{O}_{12}$ clusters from the chemisorbed layer on the Au(111) surface.

II. STM Data. The surface reconstruction of clean Au(111) is well understood (Figure 1).^{1–5} It is characterized by a 4.3% uniaxial contraction in the [110] direction. This contraction causes variations in the atomic stacking of the surface atoms so that they occupy normal fcc (having ABC stacking) and faulted hcp (having ABA stacking) regions. High-resolution helium atom scattering data were used to determine that the atoms separating the fcc and hcp regions occupy vertically displaced ($\sim 0.2 \text{ \AA}$, relative to fcc sites) bridge positions. The $\sim 0.2 \text{ \AA}$ apparent height

differential between atoms in the bridging and fcc regions was confirmed in subsequent STM studies.^{3,4} A $23 \times \sqrt{3}$ unit cell spans approximately 63 \AA along a horizontal covering 0.5 fcc–bridge–hcp–bridge–0.5 fcc sites. The pair of bridging regions contained within the $23 \times \sqrt{3}$ unit cell is manifest in STM images as elevated pairs of parallel stripes. To further reduce surface strain, the parallel bridging regions bend $\pm 120^\circ$ approximately every 250 \AA , forming the distinct Au(111) $23 \times \sqrt{3}$ herringbone pattern. A large-scale STM image of a typical clean Au sample prepared in the manner previously described displays gold terraces ranging in size from a few hundred to several thousand angstroms (Figure 4). The inset of Figure 4 shows a $400 \text{ \AA} \times 400 \text{ \AA}$ high-resolution image clearly displaying the herringbone pattern characteristic of the Au(111) $23 \times \sqrt{3}$ surface reconstruction.

Following exposure of a clean Au(111) $23 \times \sqrt{3}$ sample to 486 langmuir of $\text{H}_8\text{Si}_8\text{O}_{12}$, STM was used to image the appearance of the resultant chemisorbed layer (Figure 5). From the images, it is apparent that the Au(111) herringbone surface reconstruction is predominantly preserved, albeit with some degree of disorder (i.e., the reconstruction no longer appears as pristine following cluster exposure). Unlike all other reported molecular adsorbates having a strong chemical interaction with the Au(111) surface, chemisorption of $\text{H}_8\text{Si}_8\text{O}_{12}$ does not appear to destroy the $23 \times \sqrt{3}$ surface reconstruction. Thus, the reaction of $\text{H}_8\text{Si}_8\text{O}_{12}$ with Au(111) $23 \times \sqrt{3}$ represents the first known example in which the $23 \times \sqrt{3}$ surface reconstruction is preserved following the formation of a chemisorbed adsorbate layer. Also apparent in the STM images are numerous discontinuities and what appear to be holes present in the Au/ $\text{H}_7\text{Si}_8\text{O}_{12}$ surface (denoted by arrows labeled “1” in Figure 5b). Many of these holes form patterns of channels ~ 50 – 300 \AA in length that run parallel to each other within the adsorbate layer. Quantitative analysis of the dimensions of these features provides some qualitative information concerning the relationship between the $\text{H}_8\text{Si}_8\text{O}_{12}$ adsorbates and the underlying Au(111) $23 \times \sqrt{3}$ surface.

Recall that STM images of the clean Au(111) $23 \times \sqrt{3}$ surface display hcp and fcc regions connected by pairs of elevated stripes (i.e., bridge sites; inset, Figure 4). Cross-sectional analysis of these features yields a separation distance of $\sim 22 \text{ \AA}$ for the region between a single pair of stripes (i.e., the hcp region) and a separation distance of

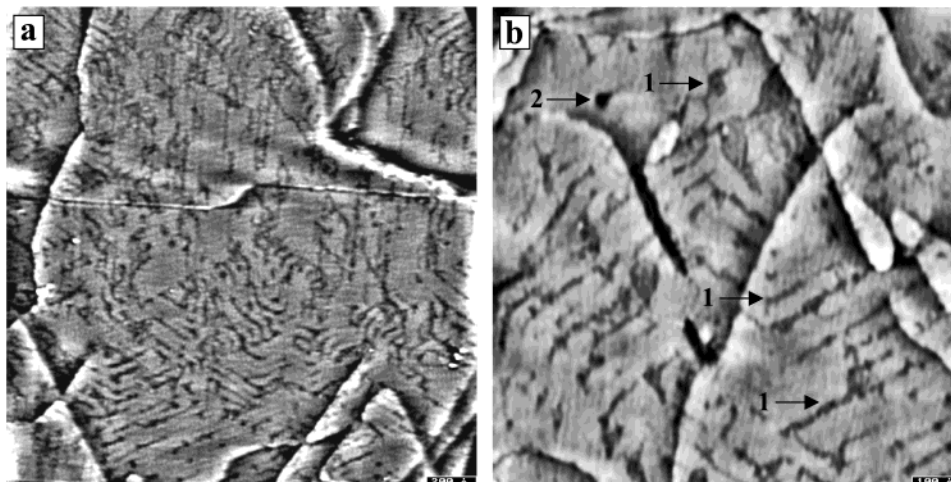


Figure 5. Au(111) sample exposed to 486 langmuir of $\text{H}_8\text{Si}_8\text{O}_{12}$: (a) $2004 \text{ \AA} \times 1998 \text{ \AA}$, $V_S = -1.01 \text{ V}$, $I_T = 2.16 \text{ nA}$; (b) $1001 \text{ \AA} \times 1001 \text{ \AA}$, $V_S = -510 \text{ mV}$, $I_T = 0.308 \text{ nA}$. These figures have been plane and slope subtracted, minimizing the vertical step height differences, to best visualize the continuity of adsorbate layer holes across individual and multiple terraces. High pass filtering was employed to attenuate extraneous noise in I_T .

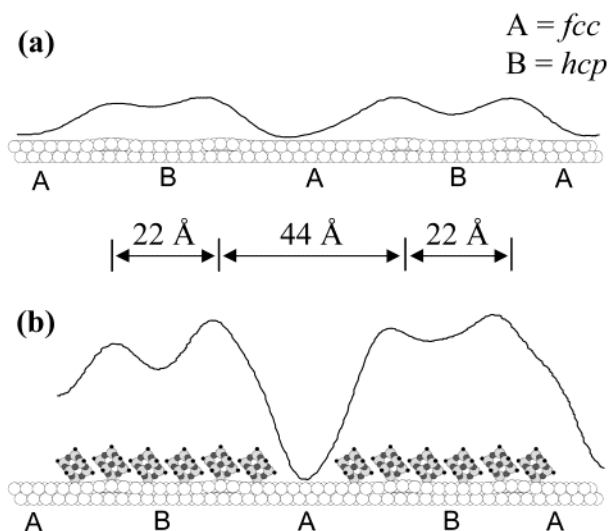


Figure 6. Side view schematics of the clean Au(111) $23 \times \sqrt{3}$ surface (a) and $H_8Si_8O_{12}$ cluster-covered Au(111) $23 \times \sqrt{3}$ surface (b). Plotted above both schematics are experimentally obtained cross-sectional profiles of the corresponding regions in STM images.

~ 44 Å for the region between pairs (i.e., the fcc region). A schematic showing a side view of two unit cells on the Au(111) $23 \times \sqrt{3}$ reconstructed surface is displayed in Figure 6a. Mapped atop the schematic is an experimental cross-sectional profile of the corresponding region in an STM image of clean Au(111) $23 \times \sqrt{3}$. The line scan clearly displays the widths of the hcp and fcc regions. An experimental cross-sectional profile spanning one adsorbate layer hole in an STM image of the Au/ $H_7Si_8O_{12}$ surface is plotted in Figure 6b. The horizontal dimensions of this region are nearly equivalent to those of the clean Au(111) $23 \times \sqrt{3}$ surface. Most noticeably, the ~ 22 Å separation distance between a single pair of “humps” and the ~ 44 Å distance spanning the adsorbate layer hole is apparent in the cross-sectional profile of Figure 6b. Interestingly, the cross-sectional profile of the Au/ $H_7Si_8O_{12}$ surface suggests that the $H_8Si_8O_{12}$ clusters are preferentially adsorbed to, and subsequently desorbed from, specific sites of the Au(111) $23 \times \sqrt{3}$ surface. Due to the preservation of the Au(111) $23 \times \sqrt{3}$ horizontal surface feature dimensions following chemisorption of $H_8Si_8O_{12}$, the STM data indicate that the $H_8Si_8O_{12}$ clusters are predominantly adsorbed to hcp and bridging regions on the Au(111) $23 \times \sqrt{3}$ surface. Additionally, the STM data indicate that $H_8Si_8O_{12}$ clusters predominantly desorb from fcc regions on the Au(111) $23 \times \sqrt{3}$ surface upon evacuation of clusters from the UHV chamber. The STM data verify the existence of holes in the chemisorbed layer of $H_8Si_8O_{12}$ clusters previously inferred from XPS and RAIRS data.^{28,29} Surprisingly, the STM data suggest that the adsorbate layer holes are predominantly located on the fcc regions of the Au(111) $23 \times \sqrt{3}$ surface.

Regions of the (a) clean Au(111) $23 \times \sqrt{3}$ and (b) Au/ $H_7Si_8O_{12}$ surfaces are displayed in Figure 7 (200 Å \times 200 Å; (a) and (b) were acquired from different samples). Two large channels in the Au/ $H_7Si_8O_{12}$ adsorbate layer, situated along fcc regions of the Au(111) $23 \times \sqrt{3}$ surface, are evident in Figure 7b. Figure 7c shows the cross-sectional profiles denoted in (a) and (b), clearly displaying an apparent height difference between similar regions on the clean Au(111) $23 \times \sqrt{3}$ and Au/ $H_7Si_8O_{12}$ surfaces. An apparent height difference of 0.9 ± 0.2 Å for the bridge regions relative to the adsorbate layer hole (i.e., fcc) regions is apparent in cross-sectional profiles of STM images of the

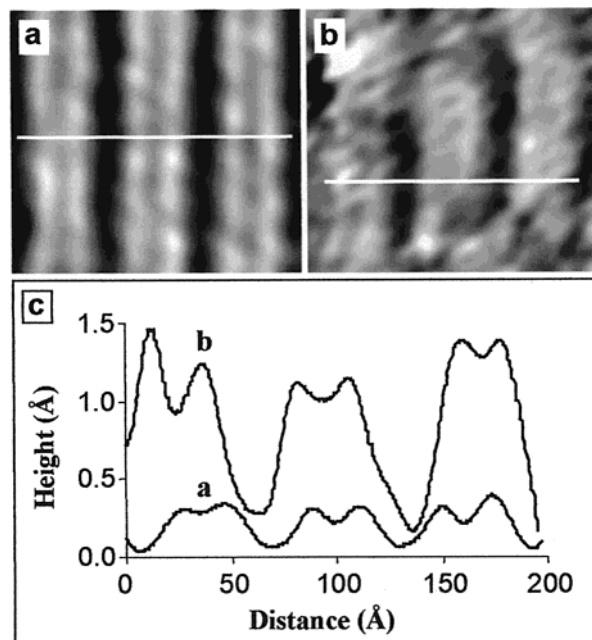


Figure 7. (a) A 200 Å \times 200 Å STM image of a clean Au(111) $23 \times \sqrt{3}$ surface; $V_S = -495$ mV, $I_T = 0.496$ nA. (b) A 200 Å \times 200 Å STM image of a Au(111) $23 \times \sqrt{3}$ surface exposed to a saturation dose of $H_8Si_8O_{12}$ (a different area from that shown in (a)); $V_S = -495$ mV, $I_T = 2.12$ nA. (c) Horizontal cross-sectional profiles of areas denoted in (a) and (b).

Au/ $H_7Si_8O_{12}$ surface. Recall that the differential in height between atoms in the bridging and fcc regions of a clean, reconstructed Au(111) surface is normally ~ 0.2 Å (as determined by high-resolution helium atom scattering and subsequent STM data; Figure 7c).²⁻⁴ Thus, the STM data indicate that the chemisorbed $H_8Si_8O_{12}$ clusters manifest themselves in the images as an additional ~ 0.7 Å in apparent height. If the clusters universally bound to all available surface sites, one would expect the addition of a uniform height distribution to all surface areas, thus preserving the ~ 0.2 Å height difference between the bridging and fcc regions. From Figure 7c, it is apparent that this is not observed in the STM data.

A three-dimensional rendering of the Au/ $H_7Si_8O_{12}$ surface dramatically displays both the lateral and vertical dimensions of the adsorbate layer features (Figure 8; 225 Å \times 225 Å). Regions of appreciable cluster coverage appear white whereas adsorbate layer holes appear black in the image. The sinuous ridges apparent in Figure 8 correspond to cluster-covered hcp and bridge sites of the underlying Au(111) $23 \times \sqrt{3}$ surface. Between the ridges, the dark regions correspond primarily to fcc sites of the underlying Au(111) $23 \times \sqrt{3}$. The 0.9 ± 0.2 Å apparent height difference between the bridging/hcp and fcc regions is clearly evident in Figure 8.

In summary, the distinct features of the Au/ $H_7Si_8O_{12}$ surface observed by STM are as follows: (1) the Au(111) $23 \times \sqrt{3}$ surface reconstruction is preserved following chemisorption of $H_8Si_8O_{12}$ clusters, (2) the $H_8Si_8O_{12}$ clusters are manifest in STM images as an additional ~ 0.7 Å in apparent height, and (3) the $H_8Si_8O_{12}$ clusters are predominantly bonded to hcp and bridging regions on the Au(111) $23 \times \sqrt{3}$ reconstructed surface.

In addition to the 0.9 ± 0.2 Å adsorbate layer holes, occasional 2.5 Å depressions are also present on the Au/ $H_7Si_8O_{12}$ surface (denoted by arrow 2 in the top portion of Figure 5b). These 2.5 Å depressions are due to small, single-step Au terraces that frequently arise as a result of the Au(111) $23 \times \sqrt{3}$ sample preparation procedure

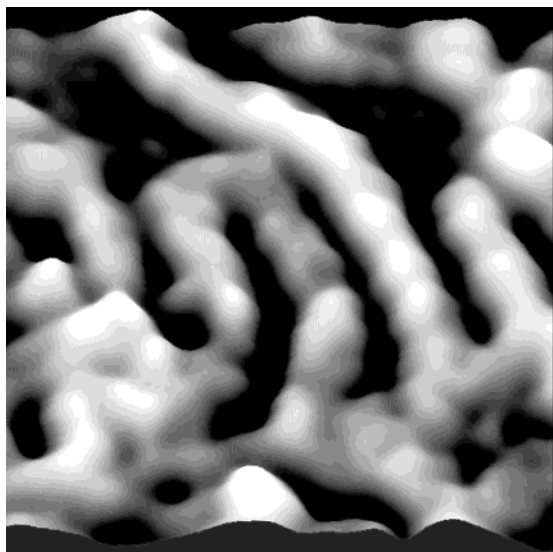


Figure 8. Height-mapped surface rendering of a Au(111) $23 \times \sqrt{3}$ sample exposed to 360 langmuir of $\text{H}_8\text{Si}_8\text{O}_{12}$; $225 \text{ \AA} \times 225 \text{ \AA}$, $V_s = -493 \text{ mV}$, $I_T = 0.225 \text{ nA}$. Low pass filtering was employed to attenuate extraneous noise in I_T .

(evident from STM images of the clean surface; Figure 4, lower right). The apparent depth of the depressed terrace suggests that it is covered with cluster adsorbates since the cross-sectional profile of a cluster-covered-to-bare-gold-terrace would give an expected depth of $\sim 3.2 \text{ \AA}$ (2.5 \AA for Au step height and 0.7 \AA apparent cluster height). The small terraces should not be confused with the formation of “vacancy islands” frequently observed for alkanethiol self-assembled monolayers on Au(111).^{6–8} Vacancy island formation caused by alkanethiol adsorption has been correlated to the lifting of the Au(111) surface reconstruction. However, recall that for the case of $\text{H}_8\text{Si}_8\text{O}_{12}$ cluster adsorbates, the Au(111) $23 \times \sqrt{3}$ surface reconstruction is *preserved* following Au/ $\text{H}_7\text{Si}_8\text{O}_{12}$ formation, thus effectively ruling out vacancy island formation.

Quantitative analysis of the STM data permits estimation of cluster coverage on the Au/ $\text{H}_7\text{Si}_8\text{O}_{12}$ surface. Normalized height histograms of typical $750 \text{ \AA} \times 750 \text{ \AA}$ STM topographs of the (a) clean Au(111) $23 \times \sqrt{3}$ and (b) Au/ $\text{H}_7\text{Si}_8\text{O}_{12}$ surfaces are plotted in Figure 9. Height histograms plot STM data in the form of pixel shade frequency versus apparent height. The STM images contain a wide range of contrast from black to white, in 4096 shades. When plotted in histogram fashion, a curve results that can be decomposed into broadened levels to indicate regions that have the same height. Integrating the individual level curves produces the surface coverage for the corresponding feature at that height. Figure 9a displays the normalized height histogram of a typical $750 \text{ \AA} \times 750 \text{ \AA}$ region of the clean Au(111) $23 \times \sqrt{3}$ surface. In this figure, brightly contrasted regions (i.e., bridge and hcp sites) have been arbitrarily set to zero. The $\sim 0.2 \text{ \AA}$ height difference between the bridge and fcc regions of the Au(111) $23 \times \sqrt{3}$ surface is readily apparent in Figure 9a. Furthermore, curve fits indicate that $\sim 65\%$ of the Au(111) $23 \times \sqrt{3}$ surface is comprised of bridge and hcp regions whereas $\sim 35\%$ of the surface is comprised of fcc regions (in excellent agreement with the surface model put forth in Figure 1). Plotted in Figure 9b is the normalized height histogram of a typical $750 \text{ \AA} \times 750 \text{ \AA}$ region of the $\text{H}_7\text{Si}_8\text{O}_{12}/\text{Au}$ surface. In this figure, bright regions (i.e., bridge and hcp sites with appreciable cluster coverage) have been arbitrarily set to zero. The $0.9 \pm 0.2 \text{ \AA}$ height difference between the cluster-covered regions

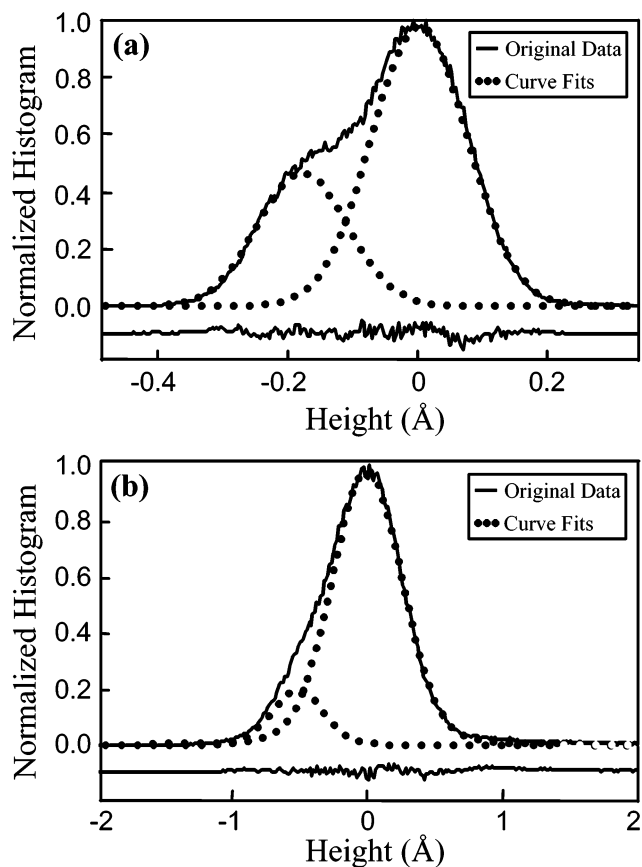


Figure 9. Normalized height histogram, with curve fit data, of typical $750 \text{ \AA} \times 750 \text{ \AA}$ STM topographs of (a) clean Au(111) $23 \times \sqrt{3}$ and (b) Au/ $\text{H}_7\text{Si}_8\text{O}_{12}$ surfaces. Analysis of curve fits taken from numerous height histograms indicates approximately $85\% \pm 5\%$ cluster coverage on the Au/ $\text{H}_7\text{Si}_8\text{O}_{12}$ surface.

and adsorbate layer holes (i.e., darkly contrasted regions) of the Au/ $\text{H}_7\text{Si}_8\text{O}_{12}$ surface is apparent. Numerous height histograms of individual terraces (necessary in order to avoid contrast contribution of ascending or descending terraces) from multiple STM images of the Au/ $\text{H}_7\text{Si}_8\text{O}_{12}$ surface were curve fit in this manner. They reproducibly show surface cluster coverage values of $85\% \pm 5\%$. Similarly, the height histograms indicate the existence of $15\% \pm 5\%$ bare gold sites in a given Au/ $\text{H}_7\text{Si}_8\text{O}_{12}$ image region, in good agreement with published estimates of $\sim 5\text{--}10\%$ based on RAIRS data.^{28,29}

III. A Chemical Test of Surface Coverage and the Presence of Adsorbate Layer Holes. Recently, the monolayer formation of $\text{C}_6\text{H}_{13}\text{-H}_7\text{Si}_8\text{O}_{12}$ clusters to a freshly evaporated Au(111) surface was reported.²⁹ However, unlike that for $\text{H}_8\text{Si}_8\text{O}_{12}$ clusters, evacuation of $\text{C}_6\text{H}_{13}\text{-H}_7\text{Si}_8\text{O}_{12}$ cluster overpressure from the UHV chamber does not produce measurable cluster desorption from the Au/ $\text{C}_6\text{H}_{13}\text{-H}_7\text{Si}_8\text{O}_{12}$ surface. $\text{C}_6\text{H}_{13}\text{-H}_7\text{Si}_8\text{O}_{12}$ clusters have been shown to displace $\text{H}_8\text{Si}_8\text{O}_{12}$ (up to $\sim 60\%$) upon exposure to the Au/ $\text{H}_7\text{Si}_8\text{O}_{12}$ surface.²⁹ Figure 10 displays the photoemission O 1s core-level spectrum of a Au/ $\text{H}_7\text{Si}_8\text{O}_{12}$ surface formed by exposure of a freshly evaporated Au(111) surface to a saturating dose of $\text{H}_8\text{Si}_8\text{O}_{12}$ (rectangles). Superimposed over the Au/ $\text{H}_7\text{Si}_8\text{O}_{12}$ spectrum, Figure 10 also displays the O 1s core-level spectrum of the Au/ $\text{H}_7\text{-Si}_8\text{O}_{12}$ surface after exposure of $\text{C}_6\text{H}_{13}\text{-H}_7\text{Si}_8\text{O}_{12}$ clusters (triangles). Integration of the respective photoemission data reveals an approximate 15% increase in O 1s core-level peak area, indicating the addition of $\sim 15\%$ oxygen-containing species to the Au/ $\text{H}_7\text{Si}_8\text{O}_{12}$ surface following exposure to $\text{C}_6\text{H}_{13}\text{-H}_7\text{Si}_8\text{O}_{12}$. Neither $\text{H}_8\text{Si}_8\text{O}_{12}$ nor $\text{C}_6\text{H}_{13}\text{-}$

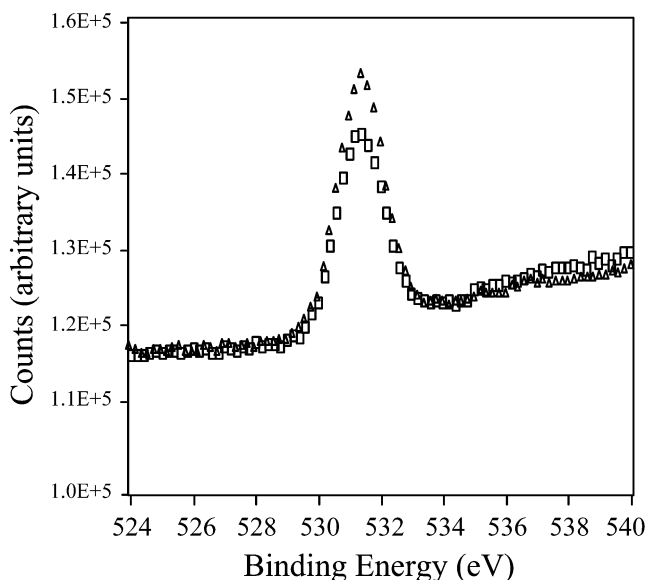


Figure 10. Conventional X-ray photoelectron spectroscopy (Mg K α) of the O 1s core levels for $\text{H}_8\text{Si}_8\text{O}_{12}$ (rectangles) and mixed $\text{H}_8\text{Si}_8\text{O}_{12}/\text{C}_6\text{H}_{13}\text{-H}_8\text{Si}_8\text{O}_{12}$ (triangles) layers on freshly evaporated gold surfaces. The data illustrate an approximate 15% difference in the integrated O 1s intensity for the $\text{H}_8\text{Si}_8\text{O}_{12}$ versus $\text{H}_8\text{Si}_8\text{O}_{12}/\text{C}_6\text{H}_{13}\text{-H}_8\text{Si}_8\text{O}_{12}$ layers.

$\text{H}_7\text{Si}_8\text{O}_{12}$ form physisorbed multilayers atop the original Au/adsorbate surface at room temperature.^{26,28,29} Therefore, the data in Figure 10 suggest that in addition to undergoing displacement reactions with $\text{H}_8\text{Si}_8\text{O}_{12}$, the $\text{C}_6\text{H}_{13}\text{-H}_7\text{Si}_8\text{O}_{12}$ clusters adsorb to the available bare gold sites present on the Au/ $\text{H}_7\text{Si}_8\text{O}_{12}$ surface. Recall that the STM data suggest the presence of $\sim 15\%$ holes in the discontinuous cluster adsorbate layer. Thus, the XPS data indicate that the $\text{C}_6\text{H}_{13}\text{-H}_7\text{Si}_8\text{O}_{12}$ clusters “fill in” the Au/ $\text{H}_7\text{Si}_8\text{O}_{12}$ adsorbate layer holes, adding an additional 15% oxygen content to the original adsorbate layer surface. The adsorbate layer holes may provide reactive sites for impinging $\text{C}_6\text{H}_{13}\text{-H}_7\text{Si}_8\text{O}_{12}$ clusters, allowing for the formation of new Au–Si bonds and the evolution of hydrogen radicals.^{28,29} The hydrogen radicals are subsequently able to react with nearby adsorbed clusters, creating a dynamic

cluster adsorption and exchange process.^{28,29} The $\sim 15\%$ increase in O 1s core-level peak intensity, consistent with $\sim 15\%$ pre-existing available surface binding sites prior to $\text{C}_6\text{H}_{13}\text{-H}_7\text{Si}_8\text{O}_{12}$ cluster introduction, is in agreement with the 5–10% $\text{H}_8\text{Si}_8\text{O}_{12}$ cluster desorption and $15\% \pm 5\%$ Au/ $\text{H}_7\text{Si}_8\text{O}_{12}$ adsorbate layer holes estimated from the RAIRS and STM data, respectively.

Conclusion

RAIRS, STM, and XPS data investigating the chemisorbed adsorbate layer formation of $\text{H}_8\text{Si}_8\text{O}_{12}$ clusters on a clean Au(111) $23 \times \sqrt{3}$ surface have been presented. All three surface characterization methods independently support desorption of approximately 10–15% of the $\text{H}_8\text{-Si}_8\text{O}_{12}$ clusters from the Au/ $\text{H}_7\text{Si}_8\text{O}_{12}$ surface following evacuation of $\text{H}_8\text{Si}_8\text{O}_{12}$ cluster overpressure from the UHV reaction chamber. The STM data are suggestive of the existence of bare surface sites following Au/ $\text{H}_7\text{Si}_8\text{O}_{12}$ adsorbate layer formation. The $\text{H}_8\text{Si}_8\text{O}_{12}$ clusters are predominantly bound to bridge and hcp sites, and preferentially desorb from fcc sites, on the Au(111) surface without significantly disrupting the $23 \times \sqrt{3}$ surface reconstruction. The reaction of $\text{H}_8\text{Si}_8\text{O}_{12}$ with Au(111) $23 \times \sqrt{3}$ represents a unique example in which the $23 \times \sqrt{3}$ surface reconstruction is preserved following the formation of a covalently bound adsorbate layer. STM experiments are currently under way to gain a better understanding of the nature of $\text{H}_8\text{Si}_8\text{O}_{12}$ cluster displacement reactions with $\text{C}_6\text{H}_{13}\text{-H}_7\text{Si}_8\text{O}_{12}$ on Au(111) $23 \times \sqrt{3}$.^{29,57}

Acknowledgment. Dow-Corning Corporation, RHK Technology, Inc., and the National Science Foundation (DMR-0093641 and DMR-9802586) are gratefully acknowledged for support of this work. Gion Calzaferri is thanked for providing a sample of $\text{C}_6\text{H}_{13}\text{-H}_7\text{Si}_8\text{O}_{12}$. Phil Holland is thanked for computer programming used in the analysis of STM topograph height histogram data. M.M.B.H. is grateful for an Alfred P. Sloan Fellowship (1999–2002). K.S.S. and D.R.F. thank the National Science Foundation for IGERT fellowships (DGE-9972776).

LA0262553

(57) Schneider, K. S.; Orr, B. G.; Banaszak Holl, M. M. In progress.